Electronic supplementary information

High-performance solution-deposited ambipolar Ir(III) complex phosphors with aggregation-induced phosphorescence enhancement behavior based on N-P=O resonant variation skeleton

Zhao Feng, [a] Hongyan Wang, [a] Siqi Liu, [a] Shipan Xu, [a] Ziyi Chen, [a] Daokun Zhong, [a] Xiaolong Yang, [a] Yuanhui Sun, [a] Guijiang Zhou [a,] *

[a] *MOE Key Laboratory for Nonequilibrium Synthesis and Modulation of Condensed Matter, School of Chemistry, State Key Laboratory for Mechanical Behavior of Materials, Xi'an Jiaotong University, Xi'an 710049, P. R. China. E-mail: zhougj@mail.xjtu.edu.cn*

Contents

General experimental information

Commercially available chemicals were used directly as received. All solvents for the reactions were dried and distilled via standard methods prior to use. The reactions were monitored using thin-layer chromatography (TLC) materials purchased from Merck & Co., Inc. Flash column chromatography and preparative TLC plates were performed with silica gel purchased from Shenghai Qingdao (300-400 mesh). ^{1}H and ^{13}C NMR spectra were recorded in $CDCl_3$ or DMSO-d_6 on a Bruker Avance 400 MHz spectrometer. Chemical shifts were referenced to the solvent residual peak at δ 7.26 ppm for ^{1}H and 77.0 ppm for ^{13}C NMR spectra in $CDCl_3$; at δ 2.50 ppm for ^{1}H NMR spectra in DMSO-d_6, respectively. UV-vis absorption spectra were recorded on a Perkin Elmer Lambda 950 spectrophotometer. Emission spectra and lifetimes for the final cyclometalated Ir(III) complexes were performed on an Edinburgh Instruments, Ltd., (FLSP 920) fluorescence spectrophotometer. Photoluminescence quantum yields (PLQYs) in solution or in doped TCTA films were measured on an Edinburgh Instruments, Ltd., (FLSP 920) fluorescence spectrophotometer with an integrating sphere. The thermal gravimetric analysis data were collected on a NETZSCH STA 409C instrument. Cyclic voltammetry (CV) was performed with a Princeton Applied Research model 273A potentiostat at a scan rate of 100 mV s^{-1}. All the CV measurements were carried out in a three-electrode compartment cell with a Pt-sheet counter electrode, a glassy-carbon working electrode, and an Ag/AgCl reference electrode. The supporting electrolyte was a 0.1 M acetonitrile solution of [nBu$_4$N]BF_4, using ferrocene as internal standard. The data of elemental analyses were acquired on a Flash EA 1112 elemental analyzer. Fast atom bombardment (FAB) mass spectra were recorded on a Finnigan MAT SSQ710 system. The HRMS data were obtained on a Waters I-class Vion IMS QTof micro-spectrometer.

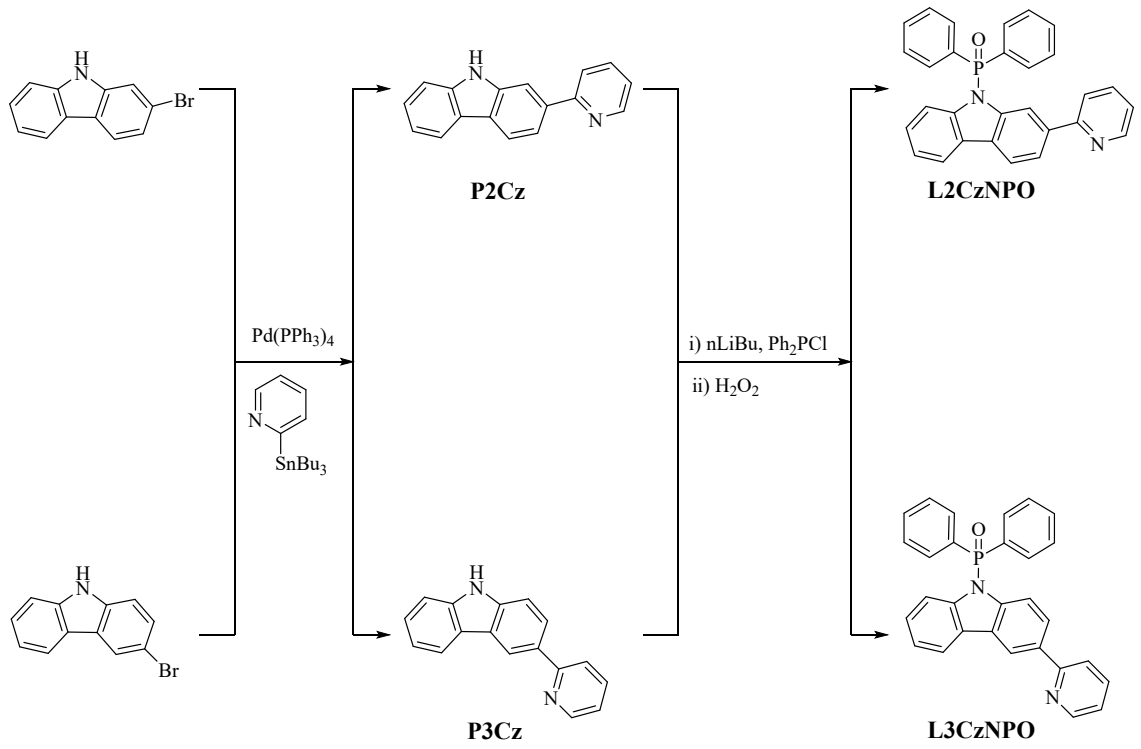

Scheme S1 Synthetic routes of the ligands **L2CzNPO** and **L3CzNPO**.

General synthetic procedure of **P2Cz** and **P3Cz**. Under a nitrogen atmosphere, to a solution of **2-bromo-9*H*-carbazole**/ **3-bromo-9*H*-carbazole** (1.0 equiv) and catalyst $Pd(PPh_3)_4$ (0.03 equiv) in toluene was dropwise added 2-(tributylstannyl)pyridine (1.1 equiv). The reaction mixture was magnetically stirred at 110 °C for 16 h. After the reaction mixture was cooled to room temperature, the solvent was evaporated to dryness under vacuum. The residue was chromatographed by a silica gel column using dichoromethane/ethyl acetate (60/1, v/v) as eluent.

P2Cz. yield: 57.3%. ^{1}H NMR (400 MHz, $CDCl_3$, δ): 8.44 (d, J = 2.0 Hz, 1H), 8.07 (dd, J = 8.8, 2.0 Hz, 1H), 7.86 (d, J = 8.8 Hz, 2H), 7.63 (d, J = 7.6 Hz, 1H), 7.46 (t, J = 7.2 Hz, 1H), 7.35 (t, J = 7.6 Hz, 1H), 7.27 – 7.25 (m, 1H), 7.22 (t, J = 7.2 Hz, 2H), 7.18 – 7.15 (m, 1H); FAB-MS (m/z): 244 $[M]^+$.

P3Cz. yield: 55.2%. ^{1}H NMR (400 MHz, DMSO-d_6, δ): 11.41 (s, 1H), 8.88 (s, 1H), 8.66 (dd, J = 4.8,

1.2 Hz, 1H), 8.22 (d, *J* = 8.0 Hz, 1H), 8.18 (dd, *J* = 8.0, 1.6 Hz, 1H), 8.05 (d, *J* = 8.0 Hz, 1H), 7.87 (t, *J* = 8.0 Hz, 1H), 7.56 (d, *J* = 8.8 Hz, 1H), 7.51 (d, *J* = 8.0 Hz, 1H), 7.41 (td, *J* = 8.0, 0.8 Hz, 1H), 7.29 (t, *J* = 5.6 Hz, 1H), 7.19 (t, *J* = 7.2 Hz, 1H); FAB-MS (m/z): 244 $[M]^+$.

General synthetic procedure of **L2CzNPO** and **L3CzNPO**. Under a nitrogen atmosphere, to a dissolved solution of **P2Cz**/**P3Cz** (1.0 equiv) in dry THF was add n-BuLi (1.2 equiv) slowly at -78 ^oC. After addition, the mixture was stirred at such a temperature for 45 min. Then, Chlorodiphenylphosphine (1.3 equiv) was added dropwise and the mixture was allowed to return to room temperature naturally. After stirring 4 h, the mixture was quenched by ice water. Subsequently, hydrogen peroxide (7.0 equiv, 33 wt% in water) was added slowly to complete the oxidation under vigorous stirring for 1 h. Finally, the mixture was extracted with dichloromethane 3 times and the organic phase was dried with anhydrous Na_2SO_4. The solvent was removed under reduced pressure and the residue was purified on a silica gel column chromatography using dichloromethane/ethyl acetate (8/1, v/v) as eluent to give the target ligands.

L2CzNPO. yield: 64.7%. ^1H NMR (400 MHz, $CDCl_3$, δ): 8.61 (dd, *J* = 4.8, 0.8 Hz, 1H), 8.11 (d, *J* = 8.4 Hz, 1H), 8.06 – 8.03 (m, 2H), 7.81 – 7.75 (m, 5H), 7.65 – 7.61 (m, 3H), 7.52 – 7.47 (m, 4H), 7.43 (d, *J* = 8.4 Hz, 1H), 7.37 (d, *J* = 8.0 Hz, 1H), 7.29 (td, *J* = 7.2, 0.8 Hz, 1H), 7.22 (td, *J* = 7.2, 1.2 Hz, 1H), 7.15 (ddd, *J* = 7.6, 4.8, 0.8 Hz, 1H); ^{31}P NMR (162 MHz, $CDCl_3$, δ): 26.37; FAB-MS (m/z): 444 $[M]^+$.

L3CzNPO. yield: 63.4%. ^1H NMR (400 MHz, $CDCl_3$, δ): 8.71 – 8.69 (m, 2H), 8.12 (d, *J* = 7.6 Hz, 1H), 7.83 – 7.73 (m, 7H), 7.63 (td, *J* = 7.2, 1.2 Hz, 2H), 7.50 (td, *J* = 7.6, 3.2 Hz, 4H), 7.37 (d, *J* = 8.4 Hz, 1H), 7.31 – 7.28 (m, 2H), 7.25 – 7.20 (m, 2H); ^{31}P NMR (162 MHz, $CDCl_3$, δ): 27.28; FAB-MS (m/z): 444 $[M]^+$.

General synthetic procedure of **Ir2CzNPO** and **Ir3CzNPO**.Under a nitrogen atmosphere, to a mixture of THF and H_2O (3/1, v/v) were added **L2CzNPO**/**L3CzNPO** (2.2 equiv) and $IrCl_3 \cdot nH_2O$ (1.0 equiv, 60 wt% Ir content). The reaction mixture was stirred at 110 °C for 16 h. After cooled to room temperature, the resultant mixture was poured into a saturated solution of NaCl. The precipitated colored Ir(III) μ-chloro-bridged dimer was obtained through filtration and dried under vacuum. Subsequently, thallium(I) acetylacetonate [Tl(acac)] (2.2 equiv) was added to an dry CH_2Cl_2 solution of the colored Ir(III) μ-chloro-bridged dimer (1.0 equiv). The reaction mixture was stirred at room temperature overnight. Centrifugation was conducted to remove the inorganic salt, and the solvent was removed under vacuum from the organic phase. The residue was purified with preparative thin-layer chromatography (TLC) made of silica gel using proper eluent. Caution: thallium(I) acetylacetonate (Tl(acac)) is extremely toxic and must be dealt with carefully.

Ir2CzNPO. yield: 32.8%. ^{1}H NMR (400 MHz, $CDCl_3$, δ): 8.56 (d, J = 5.2 Hz, 2H), 7.74 – 7.67 (m, 10H), 7.62 – 7.57 (m, 4H), 7.53 (d, J = 6.8 Hz, 2H), 7.48 – 7.42 (m, 12H), 7.18 – 7.09 (m, 4H), 7.05 – 7.00 (m, 4H), 6.76 (s, 2H), 5.22 (s, 1H), 1.78 (s, 6H); ^{13}C NMR (100 MHz, $CDCl_3$, δ): 184.63, 168.72, 148.20, 143.36, 142.03, 138.02, 137.65, 136.56, 132.86, 132.84, 132.80, 132.78, 132.33, 132.31, 132.26, 132.24, 131.77, 131.67, 130.93, 130.84, 129.00, 128.91, 128.10, 128.06, 125.91, 122.97, 121.38, 121.23, 120.07, 118.74, 114.61, 111.03, 100.55, 28.84; ^{31}P NMR (162 MHz, $CDCl_3$, δ): 25.33; MS (*m/z*) theoretical $[M+Na]^+$: 1201.2599, Found: 1201.2640;; Anal. Calcd for $C_{63}H_{47}IrN_4O_4P_2$: C, 64.22; H, 4.02; N, 4.76; found: C, 64.18; H, 4.01; N. 4.71%.

Ir3CzNPO. yield: 30.2%. ^{1}H NMR (400 MHz, $CDCl_3$, δ): 8.10 (d, J = 4.8 Hz, 2H), 8.02 (s, 2H), 7.98 (d, J = 7.6 Hz, 2H), 7.75 (d, J = 8.4 Hz, 2H), 7.69 (d, J = 8.4 Hz, 2H), 7.65 (td, J = 8.0, 1.2 Hz, 2H), 7.43 – 7.36 (m, 6H), 7.30 – 7.15 (m, 14H), 6.99 – 6.92 (m, 6H), 6.03 (s, 2H), 5.12 (s, 1H), 1.68

(s, 6H); ^{13}C NMR (100 MHz, $CDCl_3$, δ): 184.47, 167.71, 147.68, 146.08, 142.09, 141.59, 138.98, 136.41, 132.29, 132.28, 132.22, 132.21, 131.58, 131.56, 131.51, 131.49, 131.28, 130.54, 130.44, 129.72, 128.52, 128.44, 128.36, 127.48, 127.44, 125.10, 121.98, 120.88, 120.84, 119.52, 117.99, 117.89, 115.60, 115.55, 100.28, 28.57; ^{31}P NMR (162 MHz, $CDCl_3$, δ): 26.66; MS (*m/z*) theoretical $[M+Na]^+$: 1201.2599, Found: 1201.2645; Anal. Calcd for $C_{63}H_{47}IrN_4O_4P_2$: C, 64.22; H, 4.02; N, 4.76; found: C, 64.15; H, 3.99; N. 4.73%.

Theoretical computation. DFT calculations were conducted with the B3LYP method for all the final unsymmetric heteroleptic cyclometalated Ir(III) complexes. The 6-31G (d, p) basis set was applied for non-metallic C, H, O, and N atoms, while a LanL2DZ basis set for effective core potentials were employed for Ir atoms.[1, 2] Excitation behaviors were acquired by the TD-DFT calculations on the basis of the optimized ground state (S_0) geometries. Additionally, the lowest triplet state (T_1) geometries were optimized using the UB3LYP method and analysis of the natural transition orbital (NTO) was carried out for $S_0 \rightarrow T_1$ excitation. All of the calculations were performed using the *Gaussian 09* program.[3]

OLED Fabrication and Measurements. The pre-cleaned ITO glass substrates were treated with ozone for 20 min to remove residues of organic materials. Afterwards, PEDOT:PSS was spin-coated on the surface of ITO glass substrates to form a 30 nm-thick hole-injection layer and annealed at 150 °C for 15 min in the air. Then, a 25 nm-thick hole transport layer was prepared by spin-coating the chlorobenzene solution of PVK on the surface of PEDOT:PSS layer and annealed at 120 °C for 10 min in a glove box. Subsequently, spin-coating the Ir(III) complex and Tris(4-carbazoyl-9-ylphenyl)amine (TCTA) was conducted to obtained a 20 nm-thick doped TCTA region as the emissive layer. Finally, 1,3,5-tri(mpyridin-3-ylphenyl)benzene (TmPyPb) (40 nm), LiF (1 nm) and

Al cathode (100 nm) were successively evaporated at a base pressure less than 10^{-6} Torr. The EL spectra and CIE coordinates were recorded using a PR650 spectra colorimeter. The *J–V–L* curves of the devices were recorded by a Keithley 2400/2000 source meter and the luminance was measured using a PR650 SpectraScan spectrometer. All of the experiments and measurements were conducted under ambient conditions.

Notes and references

1. W. R. Wadt and P. J. Hay, Ab initio effective core potentials for molecular calculations. potentials for main group elements Na to Bi, *J. Chem. Phys.*, 1985, **82**, 284.

2. P. J. Hay and W. R. Wadt, Ab initio effective core potentials for molecular calculations. potentials for K to Au including the outermost core orbitals. *J. Chem. Phys.*, 1985, **82**, 299.

3. M. J. Frisch, G. W. Trucks, H. B. Schlegel, G. E. Scuseria, M. A. Robb, J. R. Cheeseman, J. A. Montgomery, T. Vreven Jr, K. N. Kudin, J. C. Burant, J. M. Millam, S. S. Iyengar, J. Tomasi, V. Barone, B. Mennucci, M. Cossi, G. Scalmani, N. Rega, G. A. Petersson, H. Nakatsuji, M. Hada, M. Ehara, K. Toyota, R. Fukuda, J. Hasegawa, M. Ishida, T. Nakajima, Y. Honda, O. Kitao, H. Nakai, M. Klene, X. Li, J. E. Knox, H. P. Hratchian, J. B. Cross, V. Bakken, C. Adamo, J. Jaramillo, R. Gomperts, R. E. Stratmann, O. Yazyev, A. J. Austin, R. Cammi, C. Pomelli, J. W. Ochterski, P. Y. Ayala, K. Morokuma, G. A. Voth, P. Salvador, J. J. Dannenberg, V. G. Zakrzewski, S. Dapprich, A. D. Daniels, M. C. Strain, O. Farkas, D. K. Malick, A. D. Rabuck, K. Raghavachari, J. B. Foresman, J. V. Ortiz, Q. Cui, A. G. Baboul, S. Clifford, J. Cioslowski, B. B. Stefanov, G. Liu, A. Liashenko, P. Piskorz, I. Komaromi, R. L. Martin, D. J. Fox, T. Keith, M. A. AlLaham, C. Y. Peng, A. Nanayakkara, M. Challacombe, P. M. W. Gill, B. Johnson, W. Chen, M. W. Wong, C. Gonzalez and J. A. Pople, *Gaussian 09, Revision A.2*, Gaussian, Inc., Wallingford, CT, 2009.

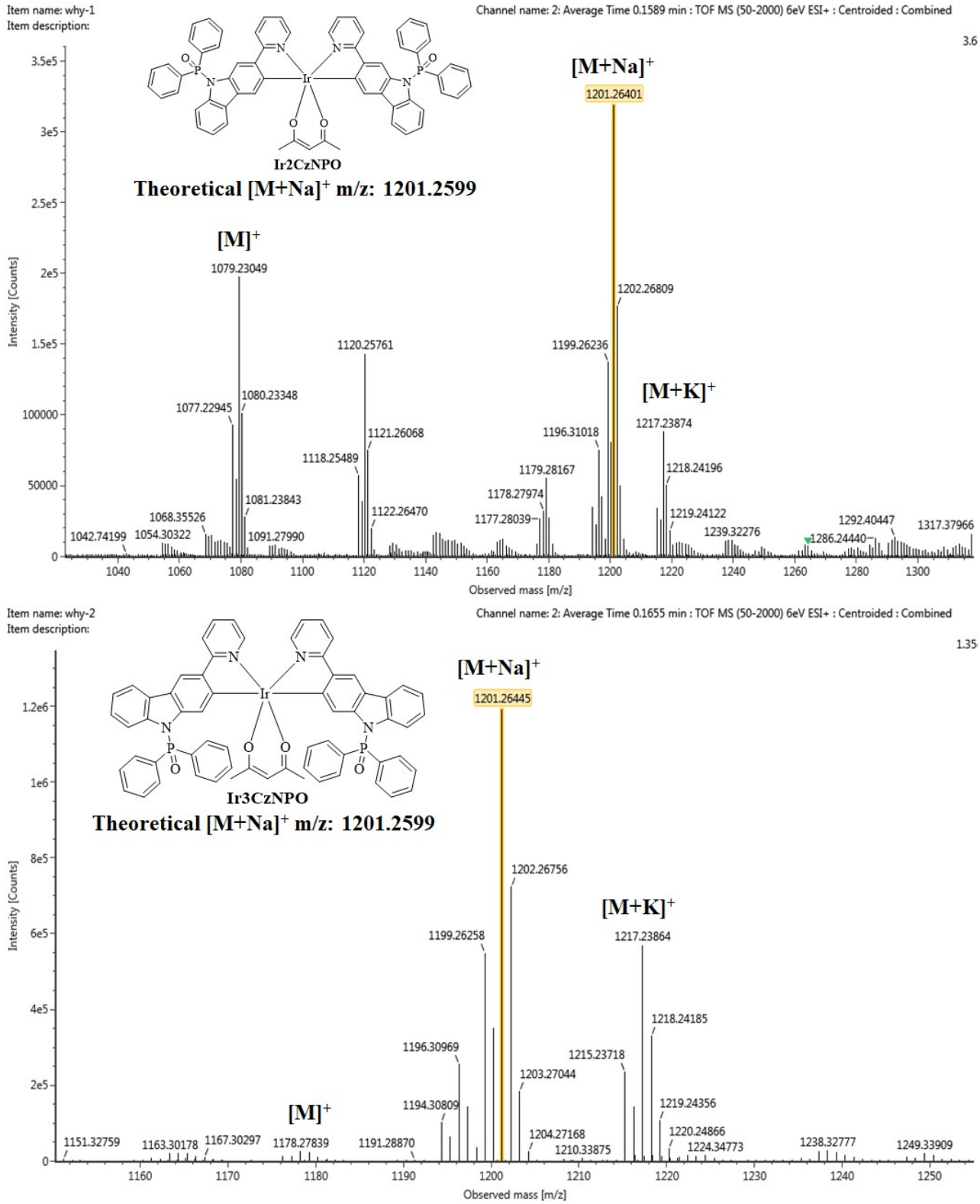

Fig. S1 High Resolution Mass Spectra (HRMS) of **Ir2CzNPO** and **Ir3CzNPO**.

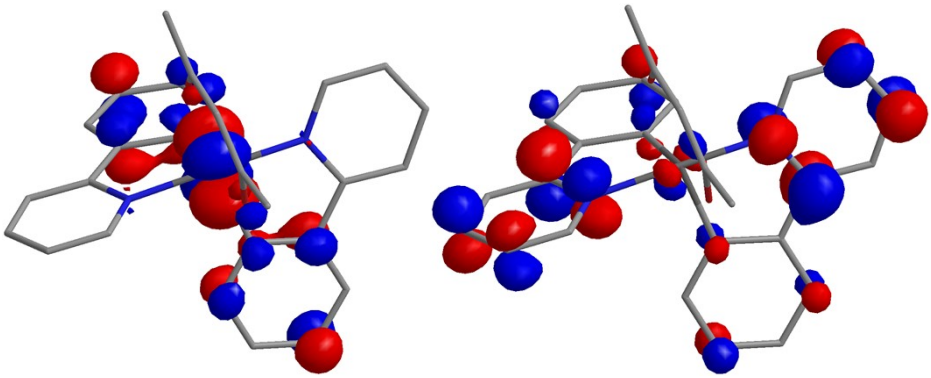

Fig. S2 HOMO (left) and LUMO (right) distribution patterns (isocontour value = 0.030) of the parental **Ir(ppy)$_2$(acac)** (**ppy** = 2-phenylpyridine) on the basis of their optimized S_0 geometries.

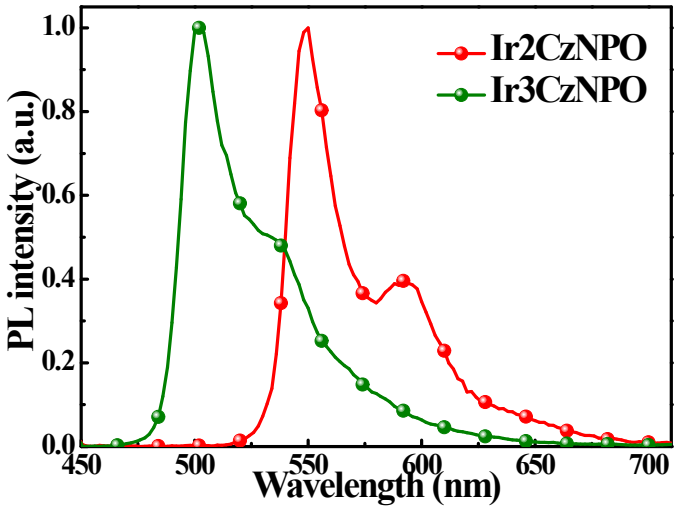

Fig. S3 Photoluminescent (PL) spectra of these carbazole-based cyclometalated Ir(III) complexes with the N-P=O resonant variation skeleton in CH_2Cl_2 solution recorded at 77 K.

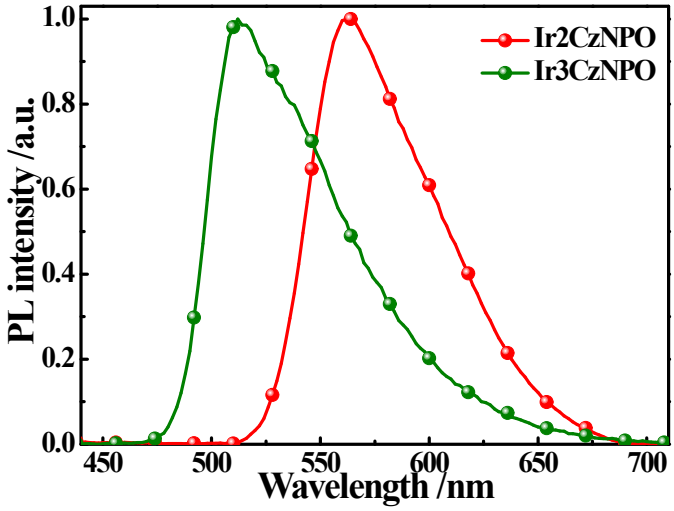

Fig. S4 Photoluminescent (PL) spectra of these carbazole-based cyclometalated Ir(III) complexes with the N-P=O resonant variation skeleton in an 8 wt% (**Ir2CzNPO**) or 4 wt% (**Ir3CzNPO**) doped TCTA film.

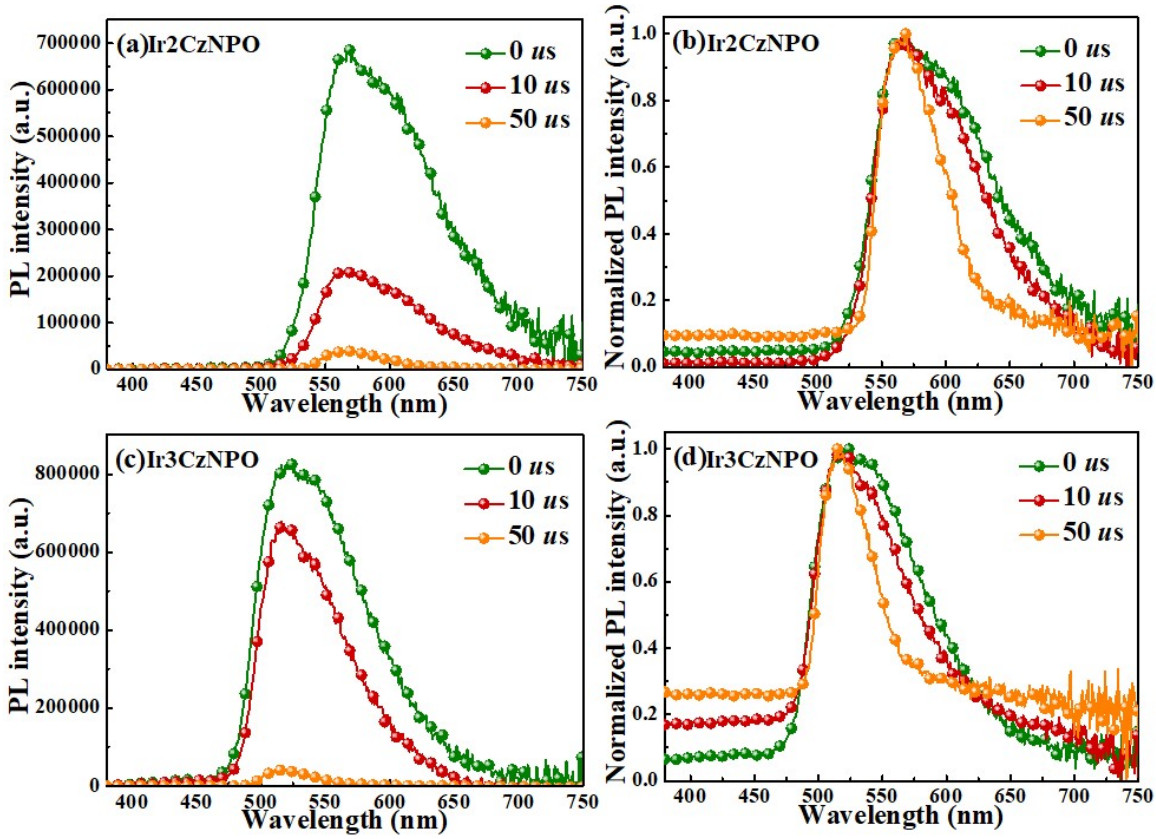

Fig. S5 Time-gated PL spectra of Ir2CzNPO (a, b) and Ir3CzNPO (c, d).

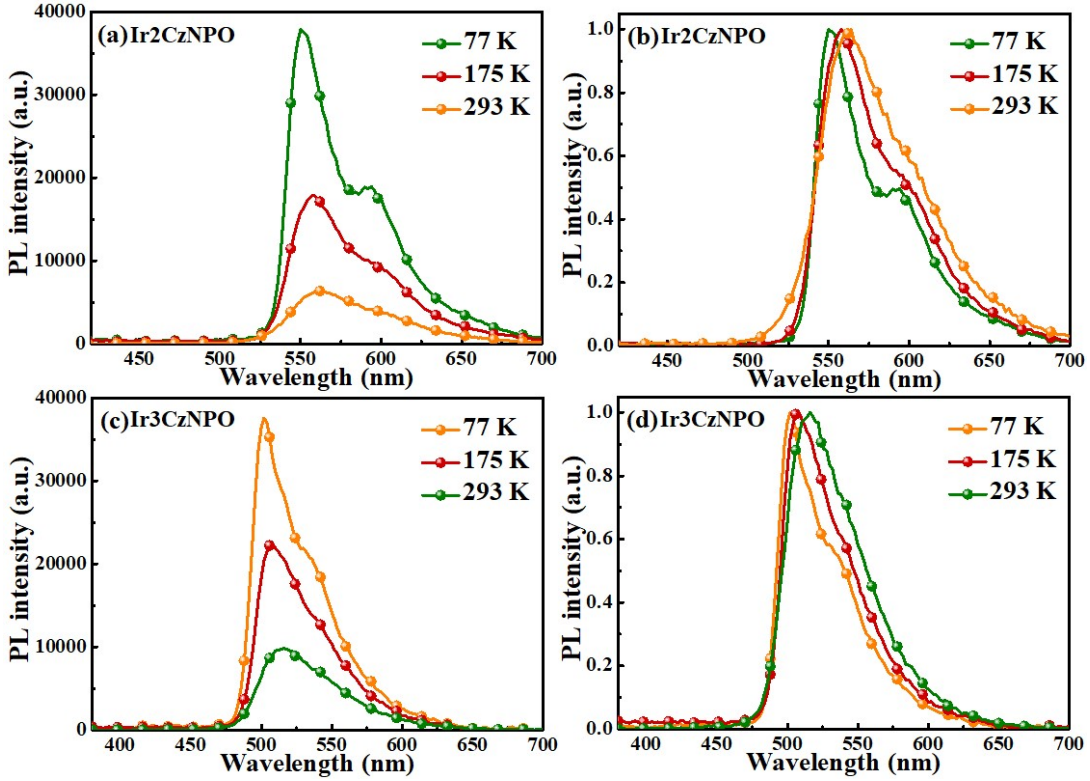

Fig. S6 Temperature-dependent PL spectra of Ir2CzNPO (a, b) and Ir3CzNPO (c, d).

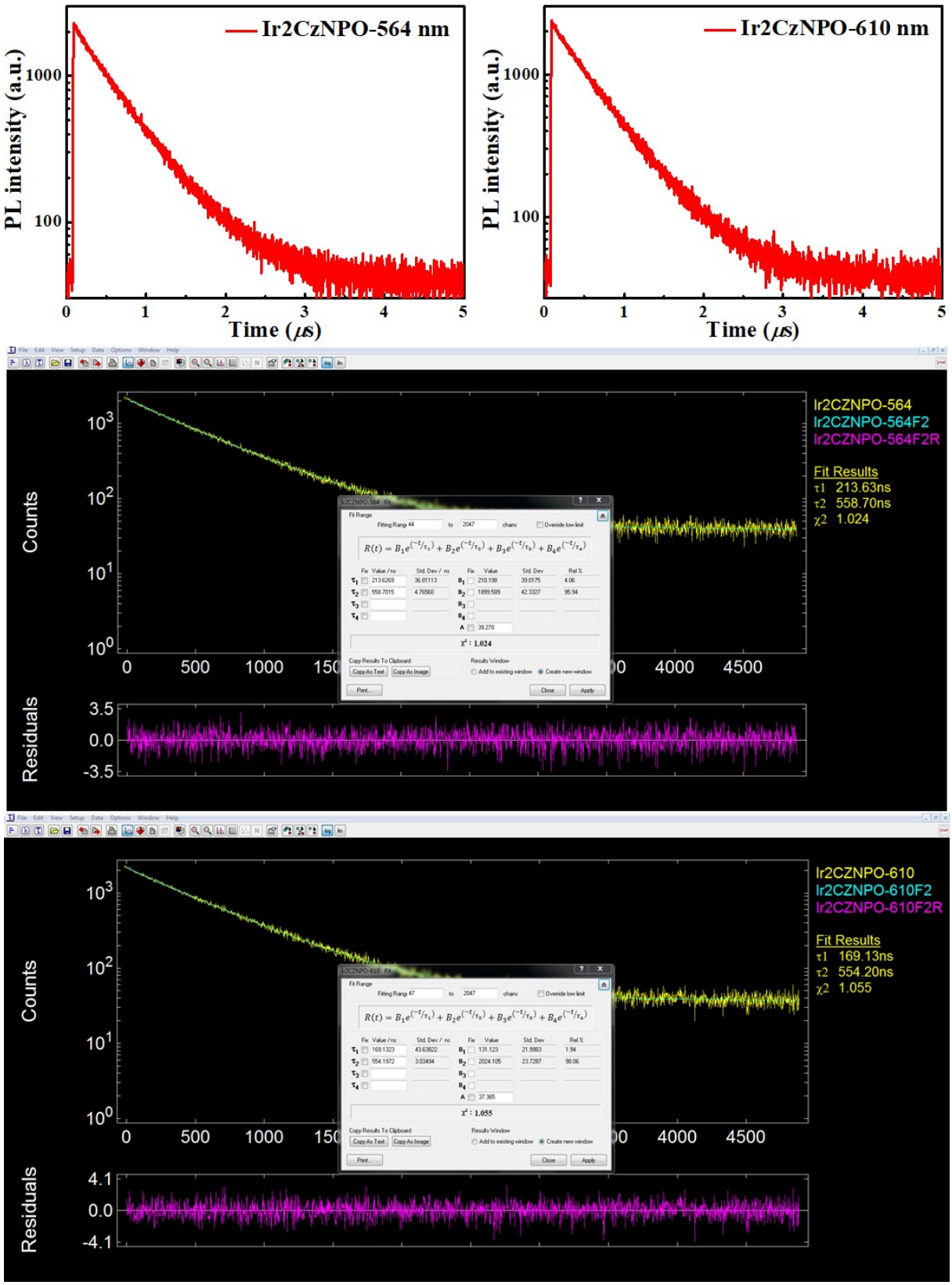

Fig. S7 Transient photoluminescence (PL) spectra of **Ir2CzNPO** in CH_2Cl_2 (*ca.* 10^{-5} M) solution under degassed condition at 293 K.

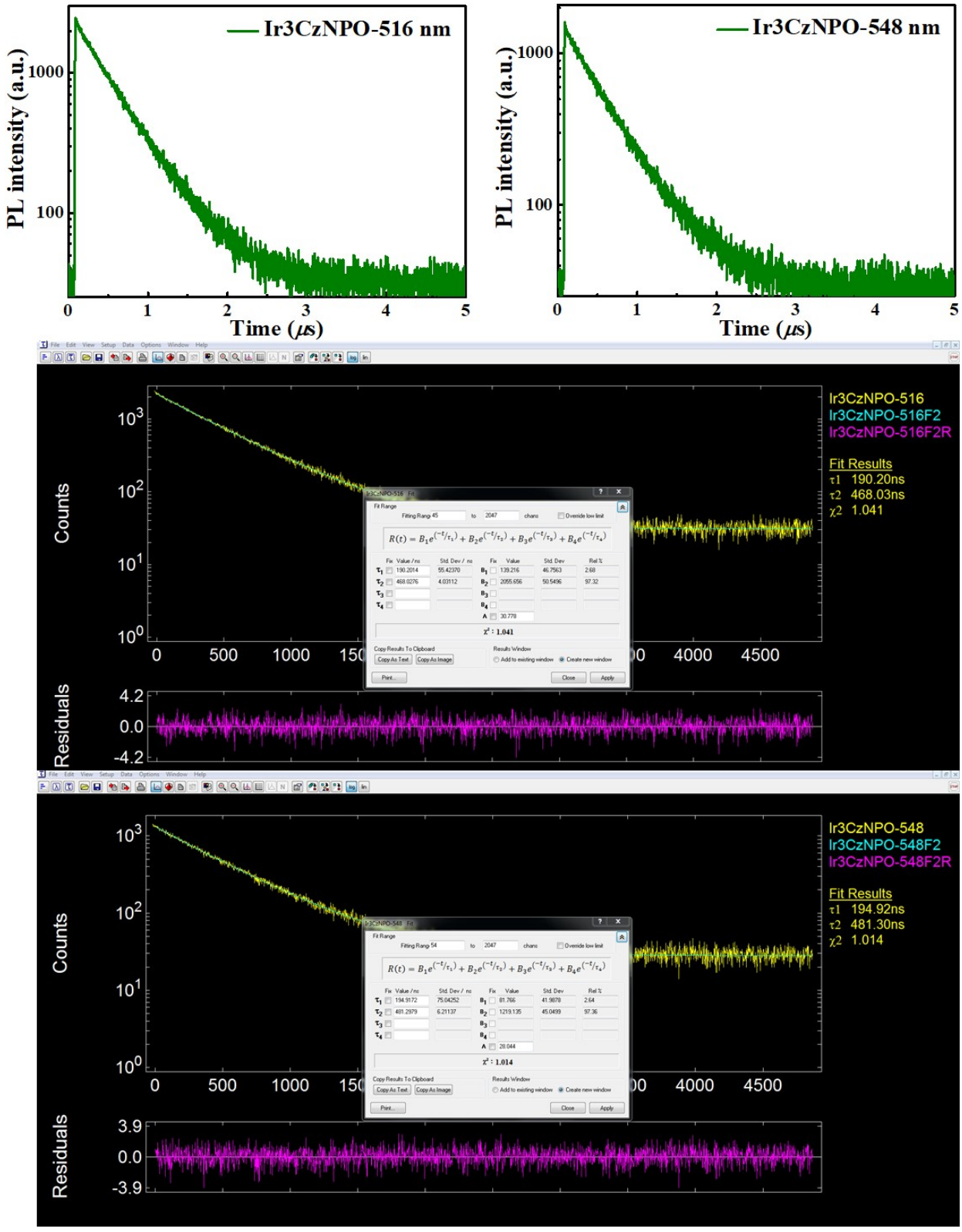

Fig. S8 Transient photoluminescence (PL) spectra of **Ir3CzNPO** in CH_2Cl_2 (*ca.* 10^{-5} M) solution under degassed condition at 293 K.

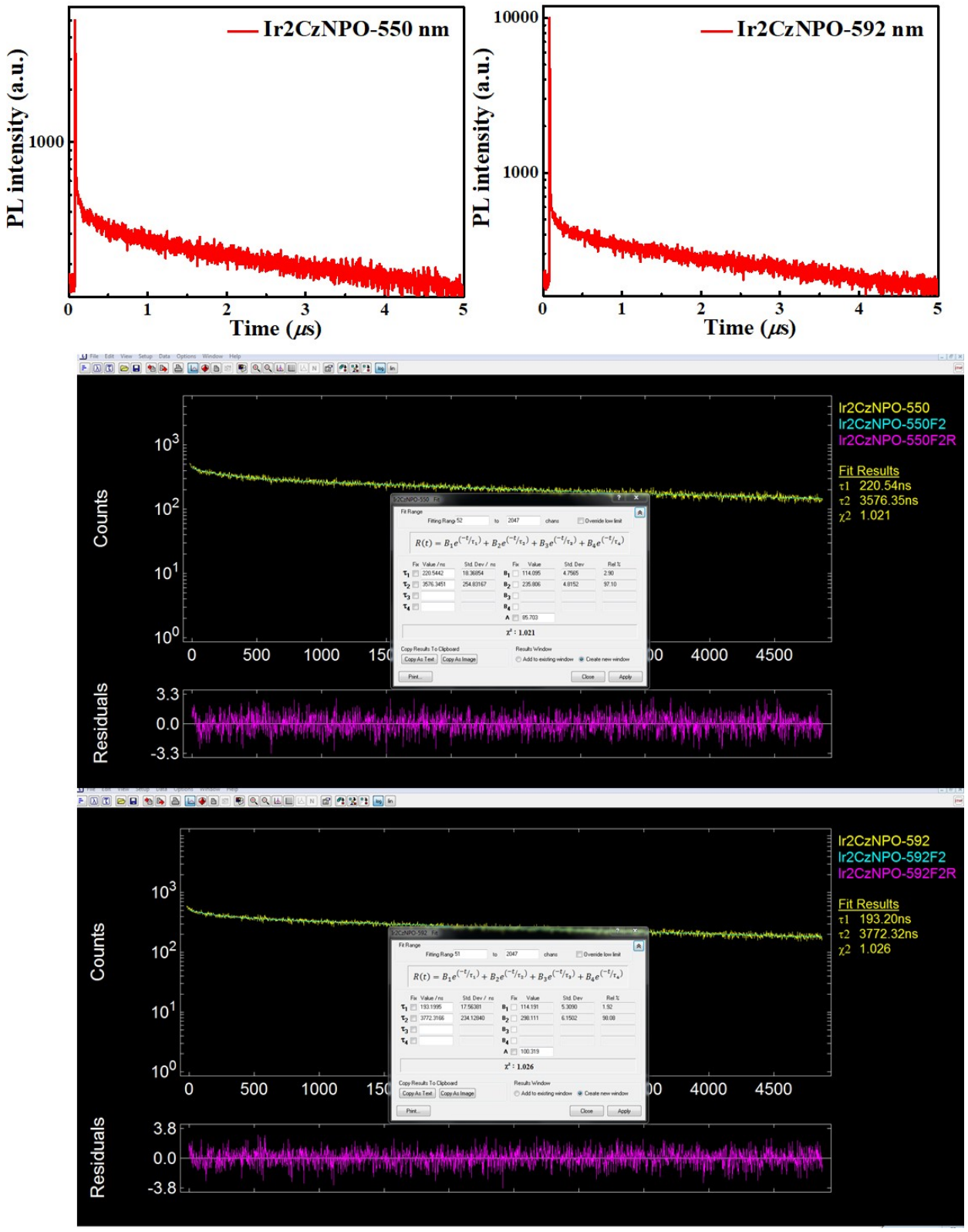

Fig. S9 Transient photoluminescence (PL) spectra of **Ir2CzNPO** in CH_2Cl_2 (*ca.* 10^{-5} M) solution under degassed condition at 77 K.

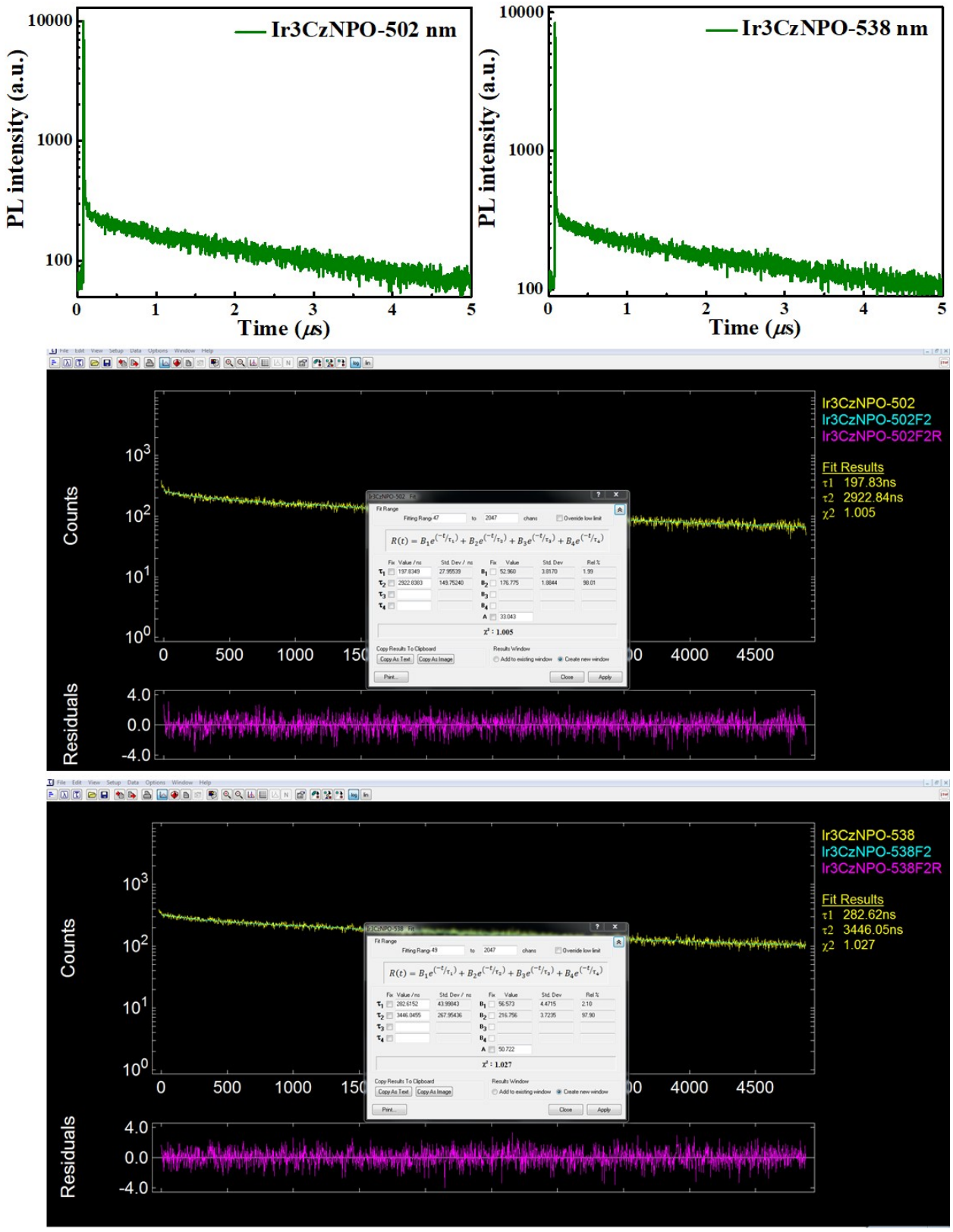

Fig. S10 Transient photoluminescence (PL) spectra of **Ir3CzNPO** in CH_2Cl_2 (*ca.* 10^{-5} M) solution under degassed condition at 77 K.

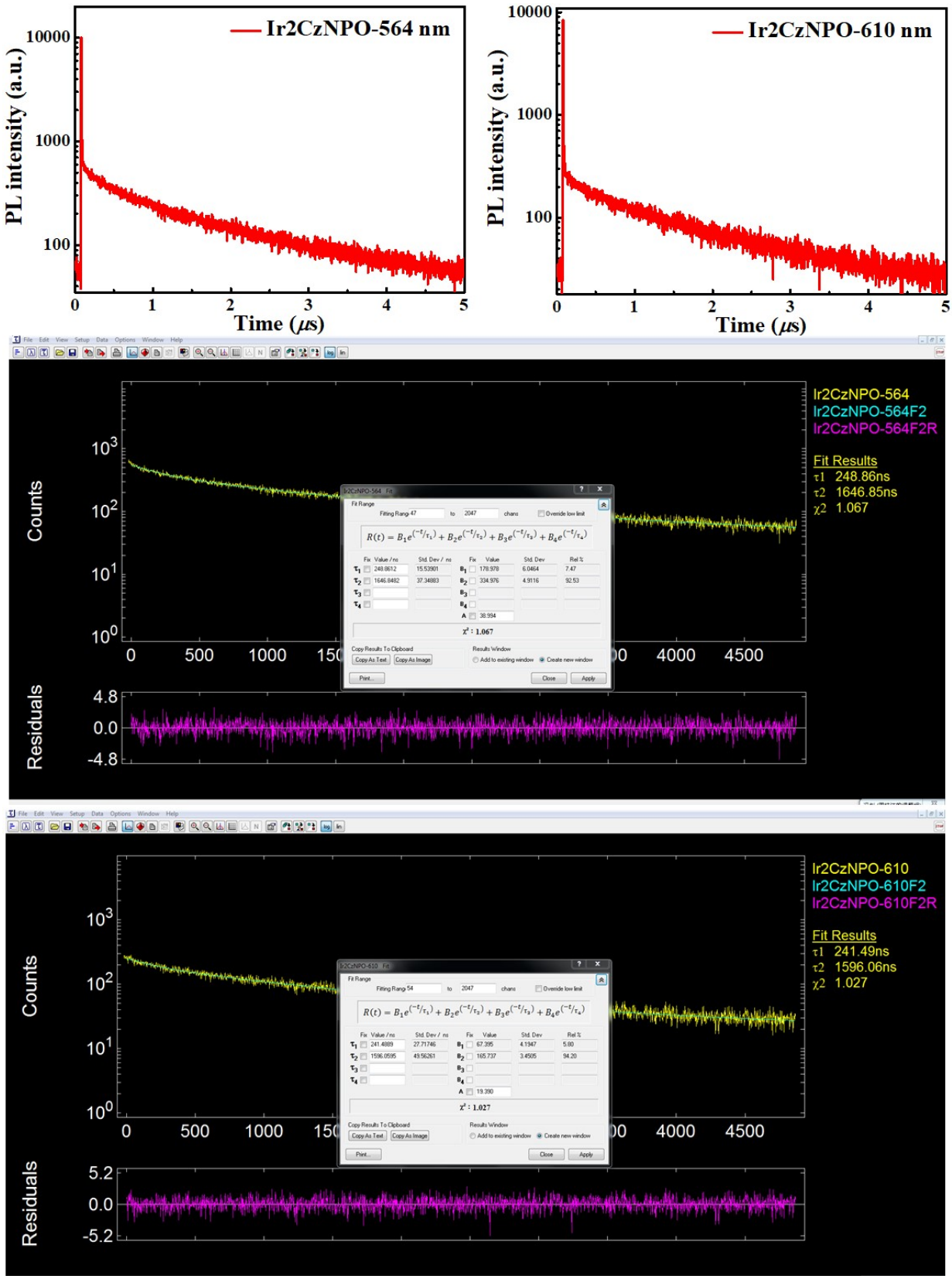

Fig. S11 Transient photoluminescence (PL) spectra of **Ir2CzNPO** in an 8 wt% doped TCTA film.

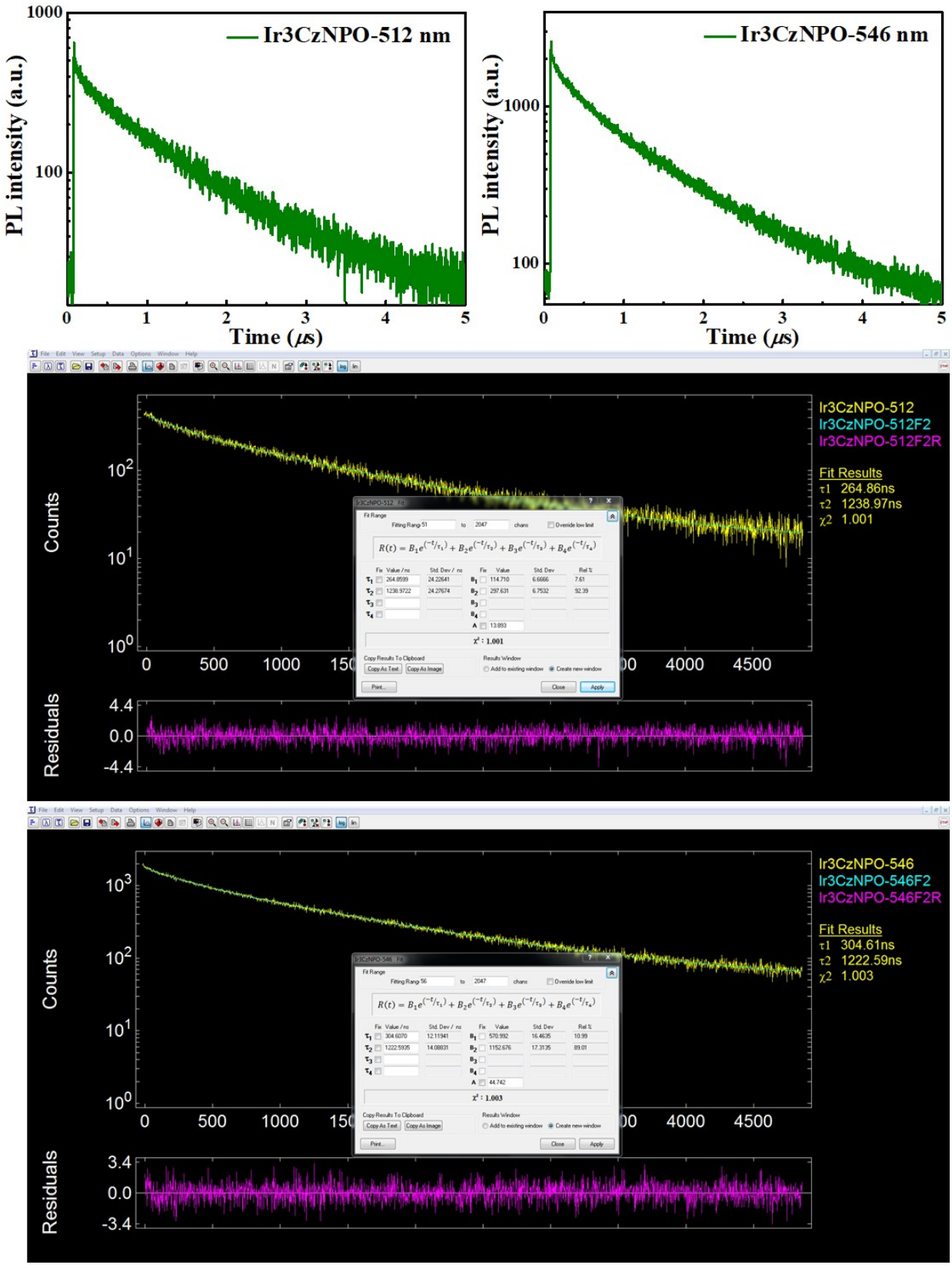

Fig. S12 Transient photoluminescence (PL) spectra of **Ir3CzNPO** in a 4 wt% doped TCTA film.

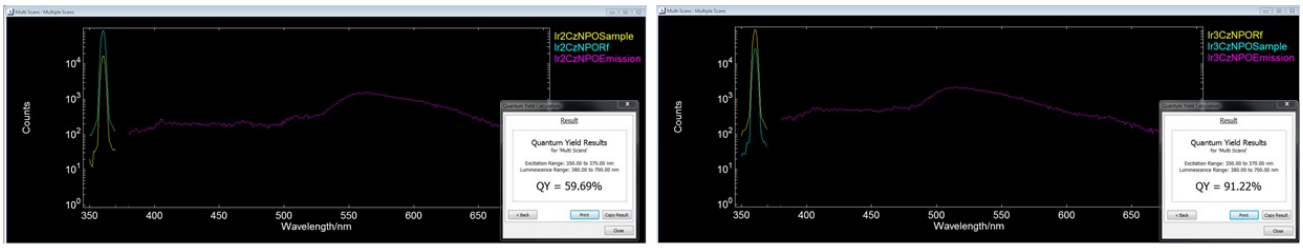

Fig. S13 PLQY of **Ir2CzNPO** (left) and **Ir3CzNPO** (right) in degassed CH_2Cl_2 solution at 293k.

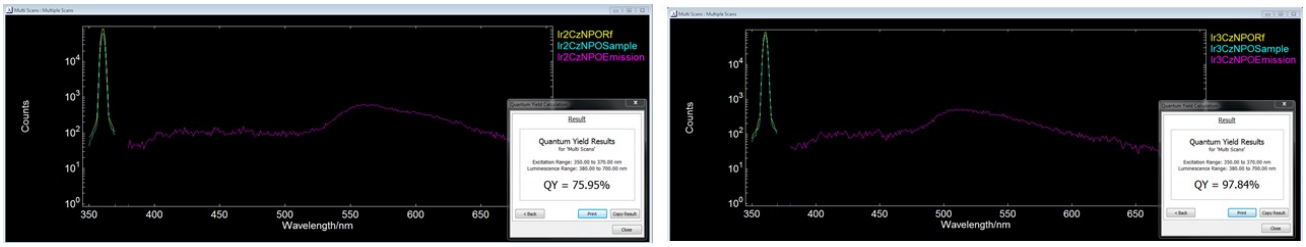

Fig. S14 PLQYs of **Ir2CzNPO** (left) in an 8 wt% doped TCTA film and **Ir3CzNPO** (right) in a 4 wt% (**Ir3CzNPO**) doped TCTA film.

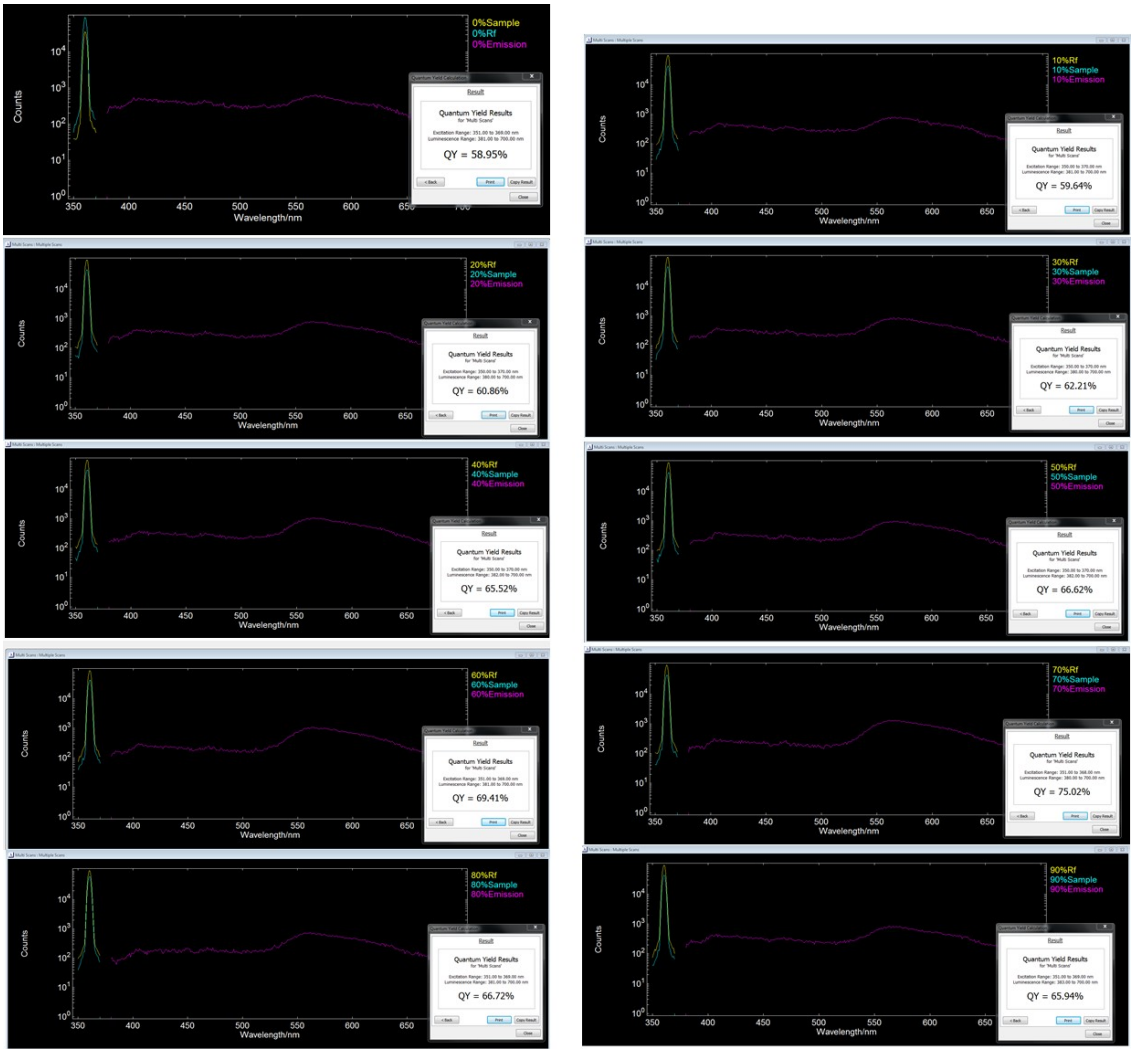

Fig. S15 PLQYs of **Ir2CzNPO** in THF/water solvent system with different f_w values under the same amount of Ir(III) complex molecules. **Ir2CzNPO** in THF solution (*i.e.* f_w = 0%) was measured at a concentration of *ca.* 10^{-5} M.

Table S1 PLQYs of **Ir2CzNPO** in THF/water solvent system with different f_w values under the same amount of Ir(III) complex molecules.

f_w	0%	10%	20%	30%	40%	50%	60%	70%	80%	90%
PLQY	58.95%	59.64%	60.86%	62.21%	65.52%	66.62%	69.41%	75.02%	66.72%	65.94%

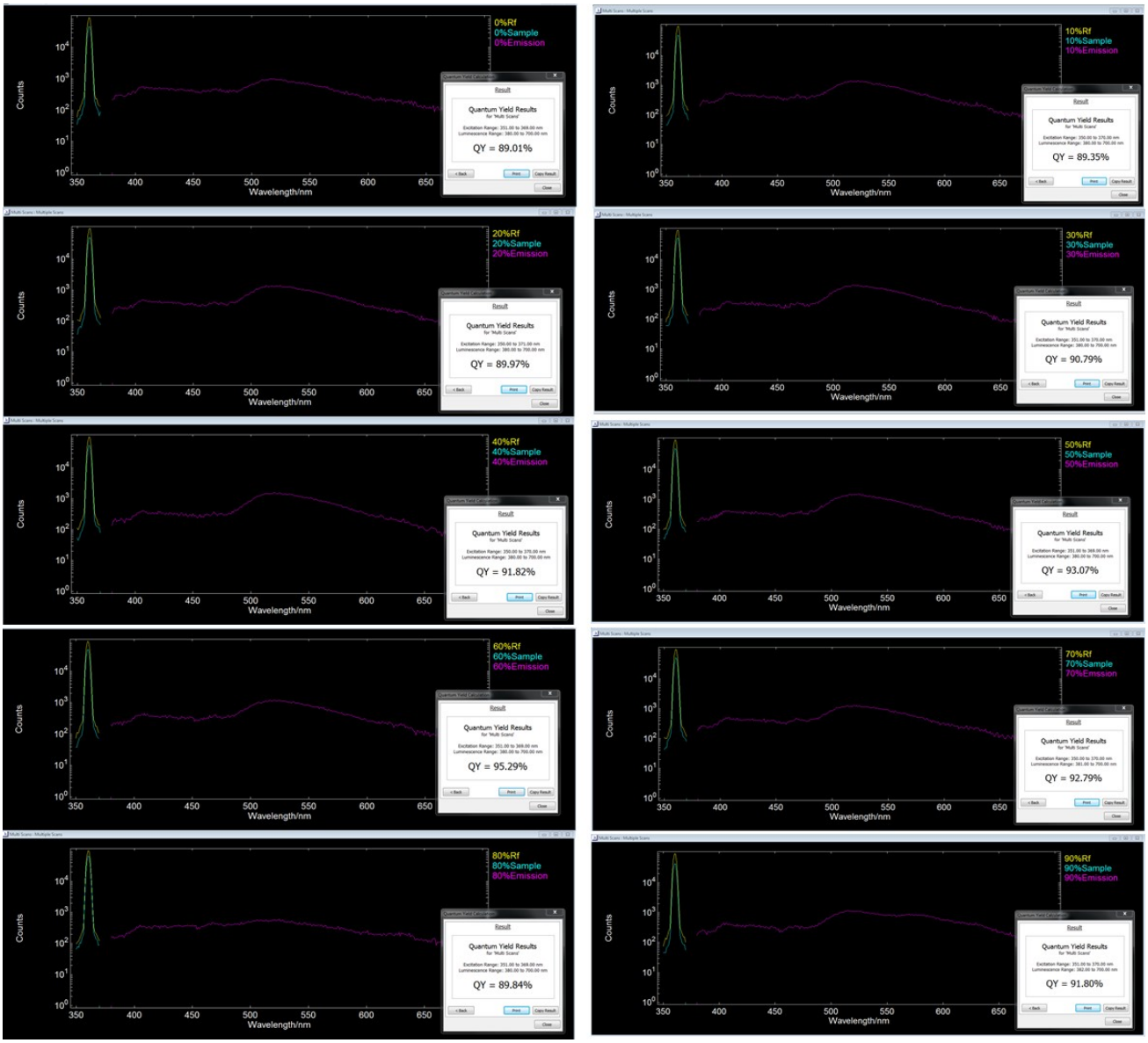

Fig. S16 PLQYs of **Ir3CzNPO** in THF/water solvent system with different f_w values under the same amount of Ir(III) complex molecules. **Ir3CzNPO** in THF solution (*i.e.* f_w = 0%) was measured at a concentration of *ca.* 10^{-5} M.

Table S2 PLQYs of **Ir3CzNPO** in THF/water solvent system with different f_w values under the same amount of Ir(III) complex molecules.

f_w	0%	10%	20%	30%	40%	50%	60%	70%	80%	90%
PLQY	89.01%	89.35%	89.97%	90.79%	91.82%	93.07%	95.29%	92.79%	89.84%	91.80%

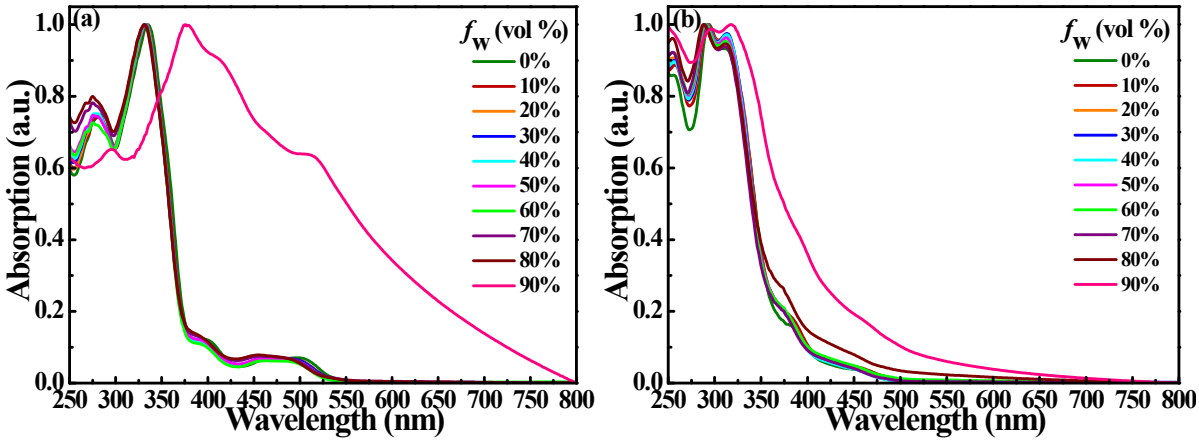

Fig. S17 UV-vis absorption spectra of **Ir2CzNPO** (a) and **Ir3CzNPO** (b) in THF/water solvent system with different f_w values under the same amount of Ir(III) complex molecules.

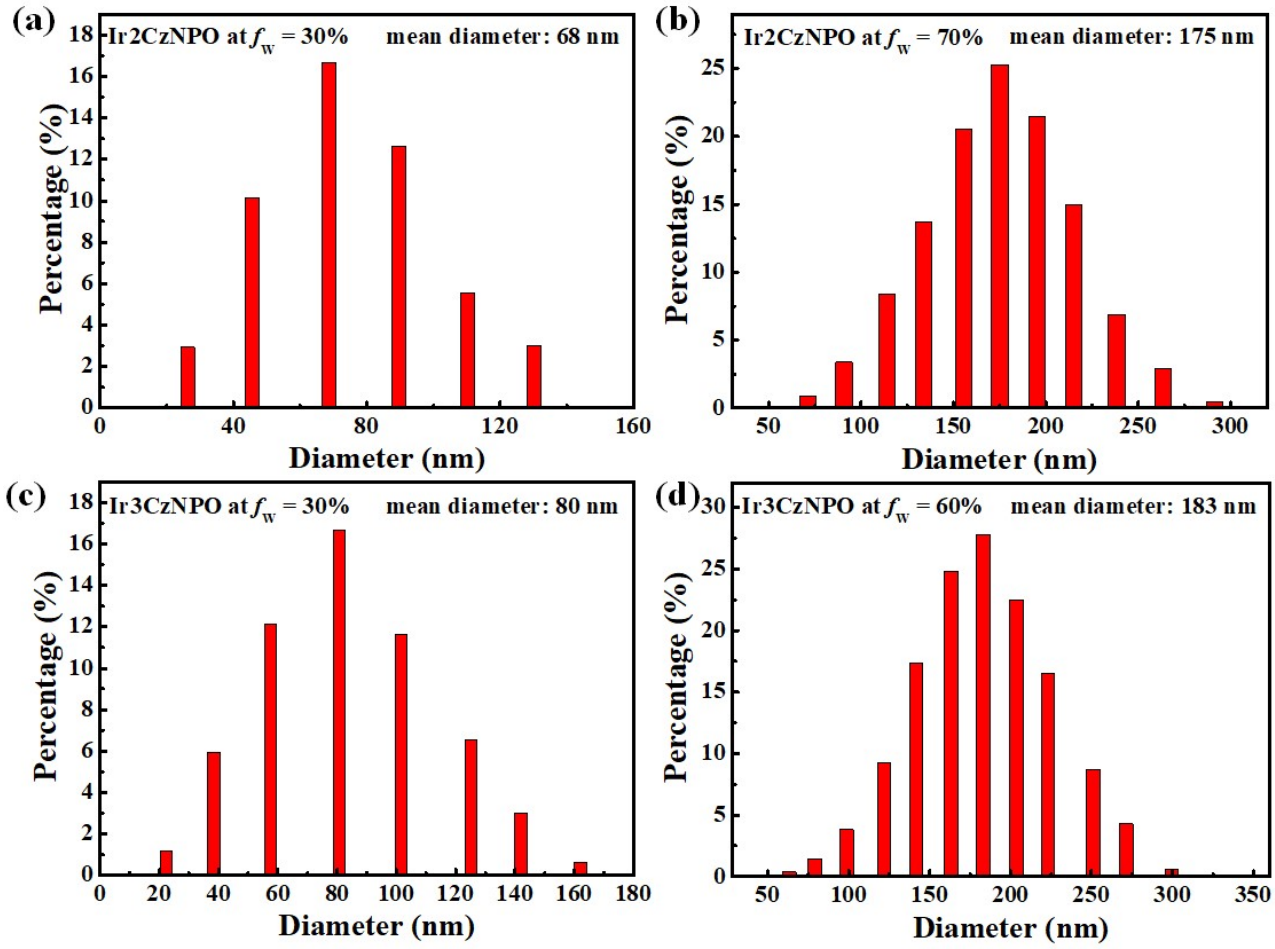

Fig. S18 Particle size distributions of **Ir2CzNPO** (a, b) and **Ir3CzNPO** (c, b) in THF/water solvent system.

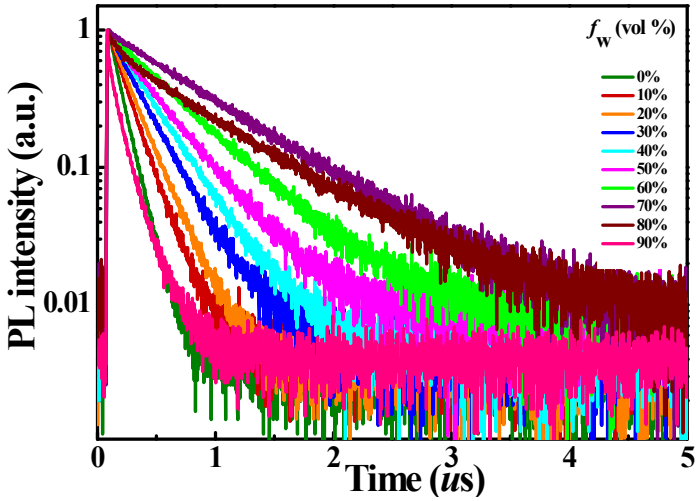

Fig. S19 Transient photoluminescence (PL) spectra of **Ir2CzNPO** in THF/water solvent system with different f_w values under the same amount of Ir(III) complex molecules. **Ir3CzNPO** in THF solution (*i.e.* f_w = 0%) was measured at a concentration of *ca.* 10^{-5} M.

Table S3 PL decay lifetime of **Ir2CzNPO** in THF/water solvent system with different f_w values under the same amount of Ir(III) complex molecules.

f_w	0%	10%	20%	30%	40%	50%	60%	70%	80%	90%
τ (*u*s)	0.12	0.17	0.20	0.27	0.323	0.395	0.53	0.80	0.77	0.134

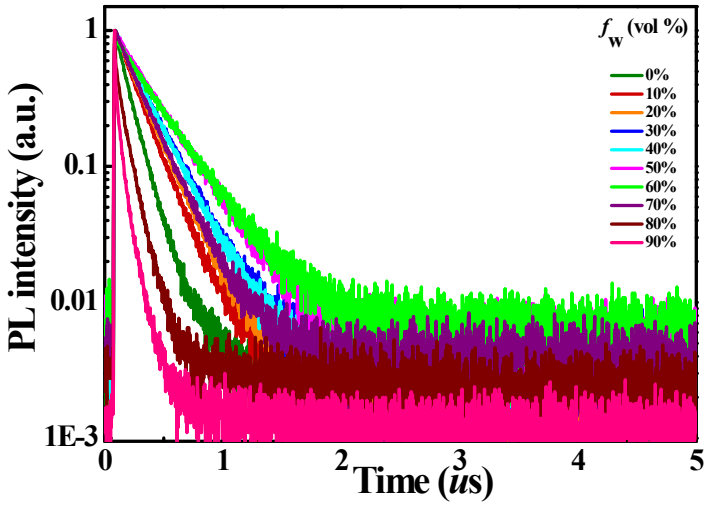

Fig. S20 Transient photoluminescence (PL) spectra of **Ir3CzNPO** in THF/water solvent system with different f_w values under the same amount of Ir(III) complex molecules. **Ir3CzNPO** in THF solution (*i.e.* f_w = 0%) was measured at a concentration of *ca.* 10^{-5} M.

Table S4 PL decay lifetime of **Ir3CzNPO** in THF/water solvent system with different f_w values under the same amount of Ir(III) complex molecules.

f_w	0%	10%	20%	30%	40%	50%	60%	70%	80%	90%
τ (*u*s)	0.14	0.19	0.21	0.24	0.26	0.31	0.33	0.22	0.09	0.07

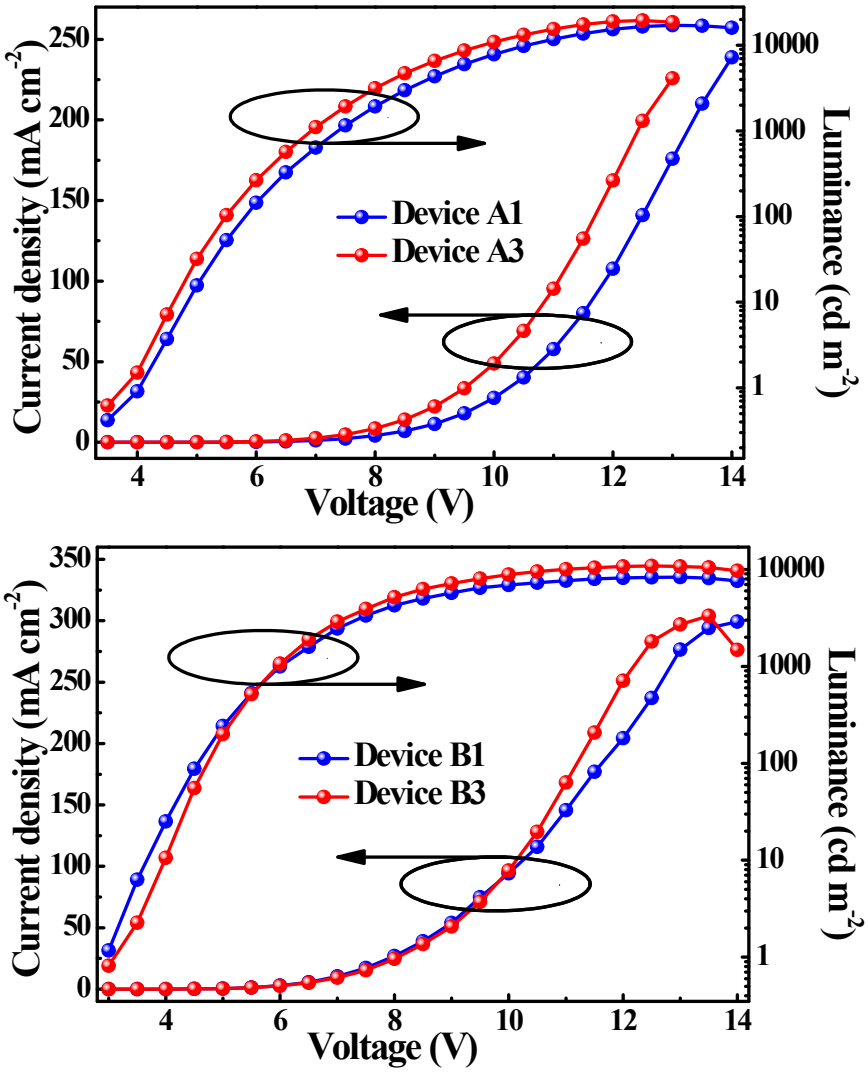

Fig. S21 Current–density–voltage–luminance (*J*–*V*–*L*) curves for the devices except the optimized ones.

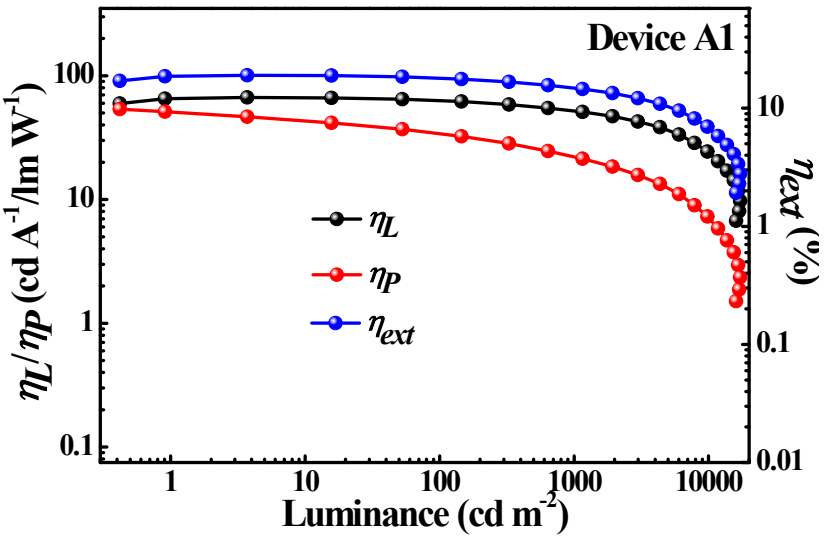

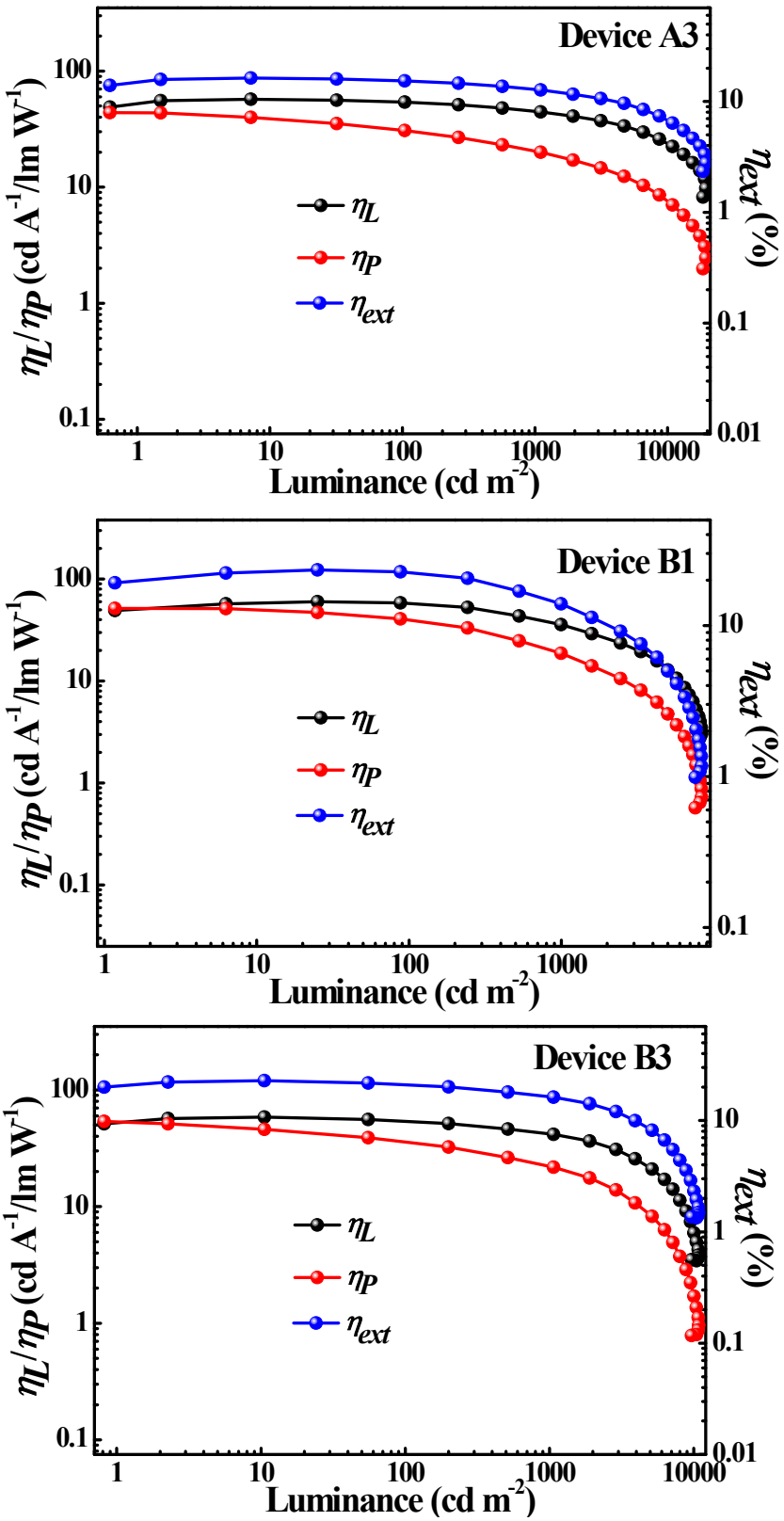

Fig. S22 Relationship between EL efficiencies and luminance for the devices except the optimized ones.

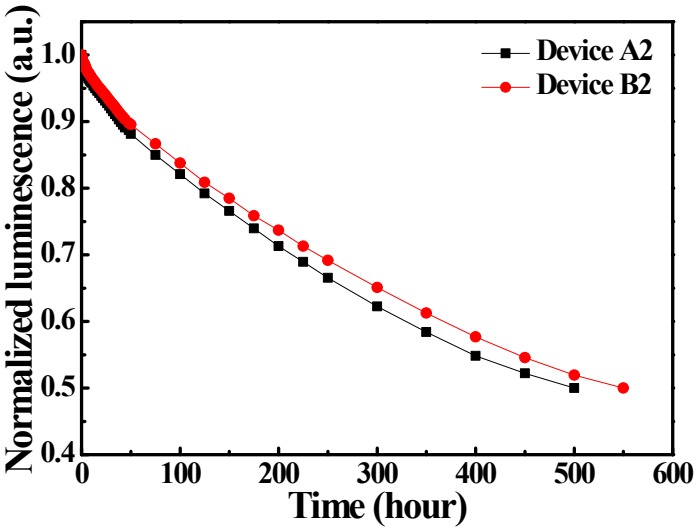

Fig. S23 Operation lifetimes of device A2 (**Ir2CzNPO**) and B2 (**Ir3CzNPO**).